Accurate Quantification and 3D Localization of Magnetic Microparticles in the Liver

Authors:

Ning Li[1,2], Cyril Tous[1,2], Ivan P. Dimov[1,2], Dominic Cadoret[1,2], Simon Lessard[2,3], Zeynab Nosrati[4], Katayoun Saatchi[4], Urs O. Häfeli[4], An Tang[1,2], Samuel Kadoury[3], Sylvain Martel[3], Gilles Soulez[1,2*]

Affiliations :

[1]Centre de recherche du Centre hospitalier de l'Université de Montréal (CRCHUM), Montréal, Québec, Canada.

[2]Department of Radiology, Radiation-Oncology and Nuclear Medicine, Université de Montréal, Montréal, Québec, Canada.

[3]Polytechnique Montréal, Montréal, Québec, Canada.

[4]University of British Columbia, Vancouver, British-Columbia, Canada.

Date: February 4, 2021

Location: Virtual seminar 2021

Département de radiologie, radio-oncologie et médecine nucléaire
Faculté de médecine
Université de Montréal

Disclosures

This work was supported by a grant from the Natural Sciences and Engineering Research Council of Canada (NSERC), Operating Grant - CHRP (CIHR Partnered) (CHRP 478474-15), Canadian Institutes of Health Research (CIHR), Operating Grant - CHRP (NSERC Partnered) (CPG-140179), Fonds de recherche du Québec en Santé (FRQS) and Fondation de l'association des radiologistes du Québec (FARQ) Clinical Research Scholarship (34939), Transmedtech and Siemens Healthineers. We also acknowledge support by the Lundbeck Foundation of Denmark (UBC-SUND Lundbeck Foundation Professorship to UOH, No. 2014-4176).

1. Introduction

Serious situation (Worldwide)

Liver cancer, the second leading cause of cancer-induced death. Hepatocellular carcinoma (HCC) makes up approximately 80%-90% of all cases of primary liver cancer.

lung (1.59 million deaths)
liver (745 000 deaths)
stomach (723 000 deaths)
colorectal (694 000 deaths)
breast (521 000 deaths)

World Health Organization

Treatment methods and problems

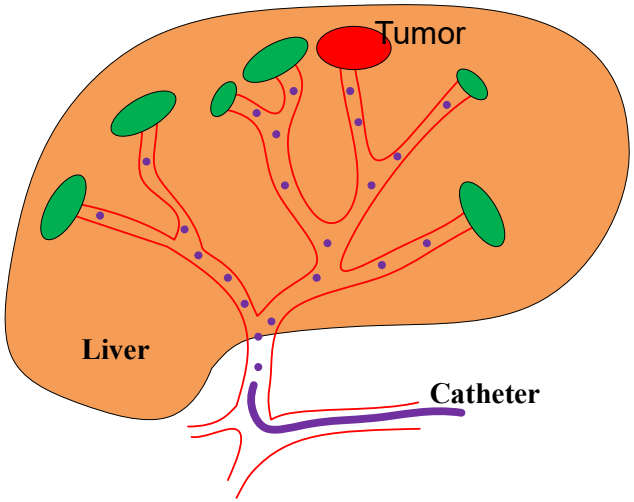

Transcatheter arterial chemoembolization

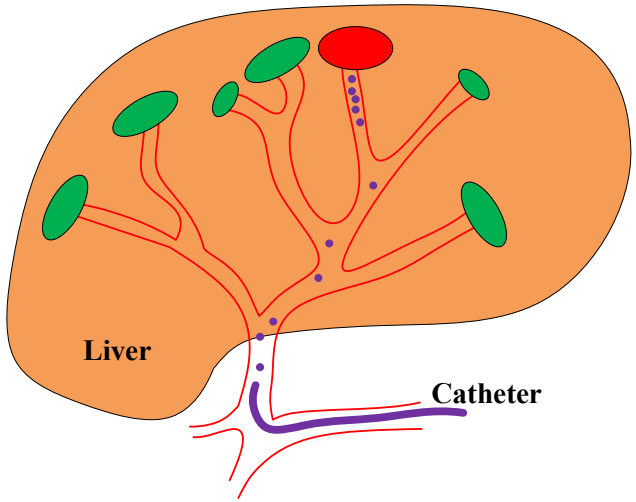

MR tracking + MR steering + Flow drifting = Magnetic resonance navigation （MRN） of magnetic drug-eluting beads (MDEBs)

Accurate quantification and 3D localization of MDEBs in vivo

?

2. Method

2.1 Synthesizing, injecting and imaging MDEBs

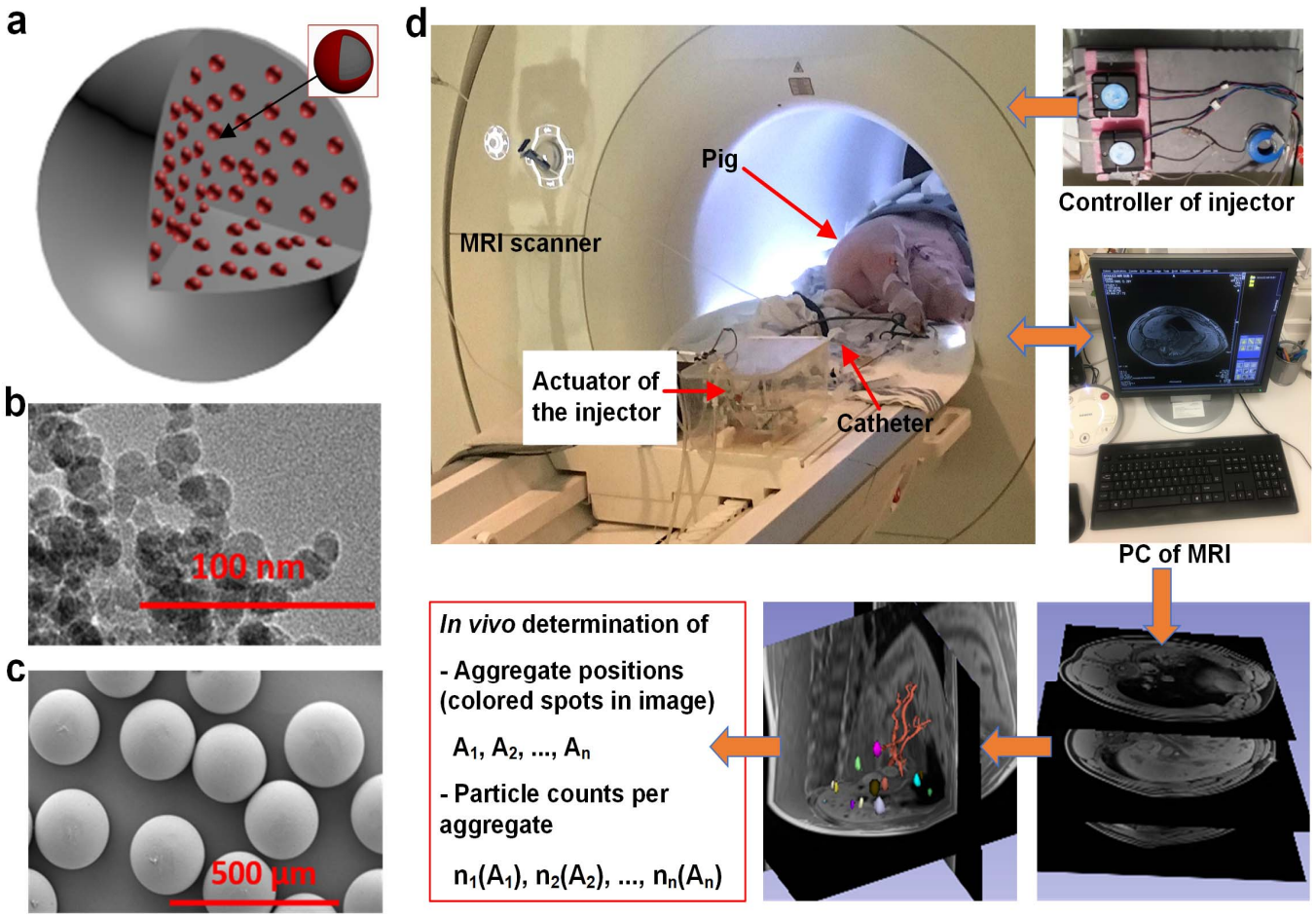

Synthesizing, injecting and imaging MDEBs. a) Schematic diagram of the synthesized PLGA-based-MDEB encapsulating Fe_3O_4 nanoparticles coated with C_{12}-bisphosphonate. **b)** Transmission electron microscopy (TEM) micrograph of the Fe_3O_4 nanoparticles. **c)** Scanning electron microscope (SEM) image of MDEBs. **d)** Schematic representation of the workflow. The catheter, inserted into the hepatic artery of the pig, was connected to the MRI-compatible injection system to allow the injection of MDEB aggregates into the proximal proper hepatic artery. The proposed analysis method, based on the T1-VIBE-based susceptibility artifact reconstruction, was used to quantify and locate MDEB aggregate fragments located throughout the liver.

2. Method

2.2 Choosing the proper MR imaging sequence

Two main criteria: the **acquisition time** (a short acquisition time compatible with a breath hold and a good spatial resolution) and **the size of the artifact** (a large artifact may create an overlap of signal loss induced by individual MDEB aggregates thus limiting aggregate).

Acquisition time

1) T1 VIBE sequence (out-of-phase (OP): TR = 5.2 ms, TE = 1.4 ms ; in-phase (IP): TR = 5.2 ms, TE = 2.6 ms, BW = 1040 Hz, slice thickness = 3 mm, pixel resolution = 320, slice = 72**,** ***time acquisition (TA) = 19 s***)

2) T2 sequence (same parameters with changes on TR = 1000 ms, TE = 72 ms, ***TA = 10 min 49 s***)

3) T2* sequence (same parameters with changes on TR = 650 ms, TE = 18 ms, ***TA = 7 min***)

The size of the artifact

A single particle was clearly visible in the PVA phantom aggregates using T1 VIBE sequence without large susceptibility artifact thus minimizing the risk of overlap between individual areas of signal loss.

2. Method

2.3 How to calculate the artifact volume of a MDEB aggregate & Proposing the model to build the relationship between the particle count and the voxel count

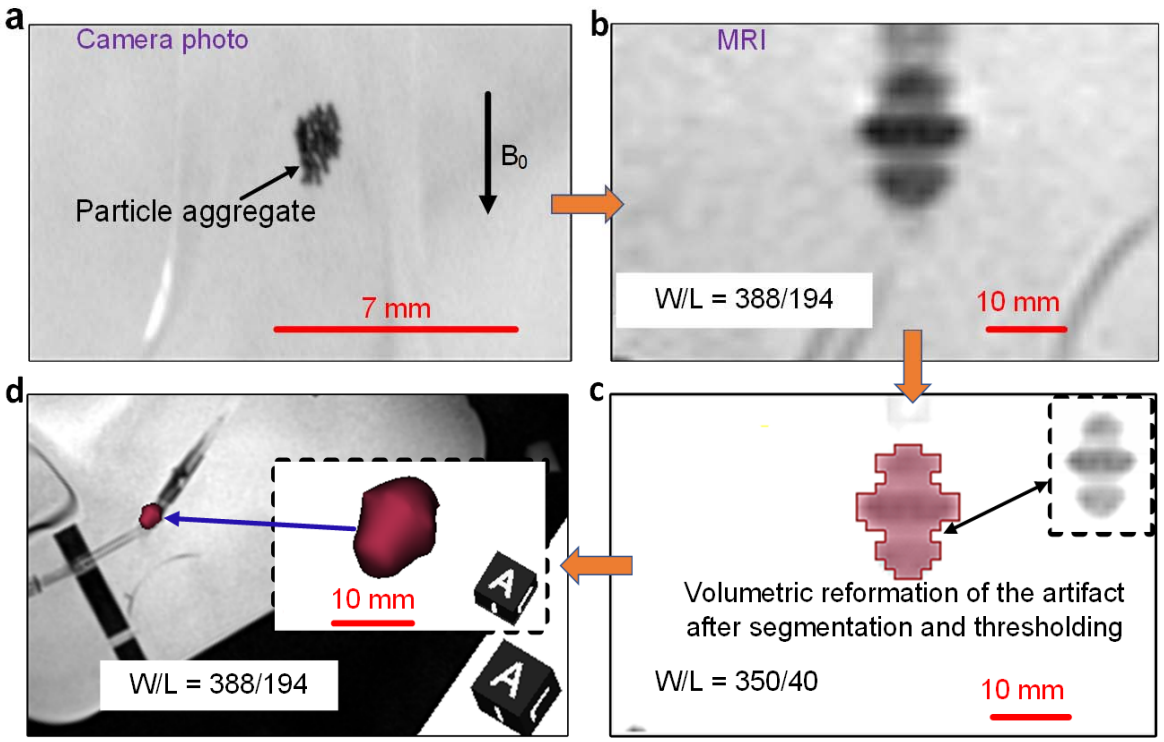

Flowchart showing how to obtain the artifact volume from MR imaging. a) Photograph of a 60-particle aggregate in the glass phantom inside the MRI bore. **b)** MR imaging of the aggregate artifact. **c)** Segmentation of the aggregate artifact using the analysis software, 3D-SLICER. **d)** 3D reformation of aggregate segmentation.

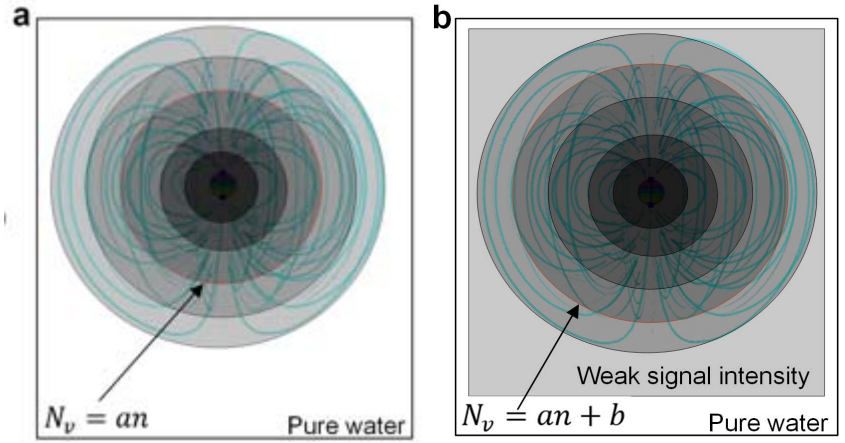

A sketch to show the different relationships between the particle count and the voxel count without (a) and with (b) weak signal intensity.

Note: N_v is the voxel count, n represents the object volume, and the parameter a is a constant ratio which is determined by the imaging parameters (BW, TE, B_0), and b is a noise signal which relies on the signal intensity of objects surrounding the MDEBs.

3. Results

3.1 *In vitro* testing of the relationship between the particle count and the artifact voxel count in a glass phantom

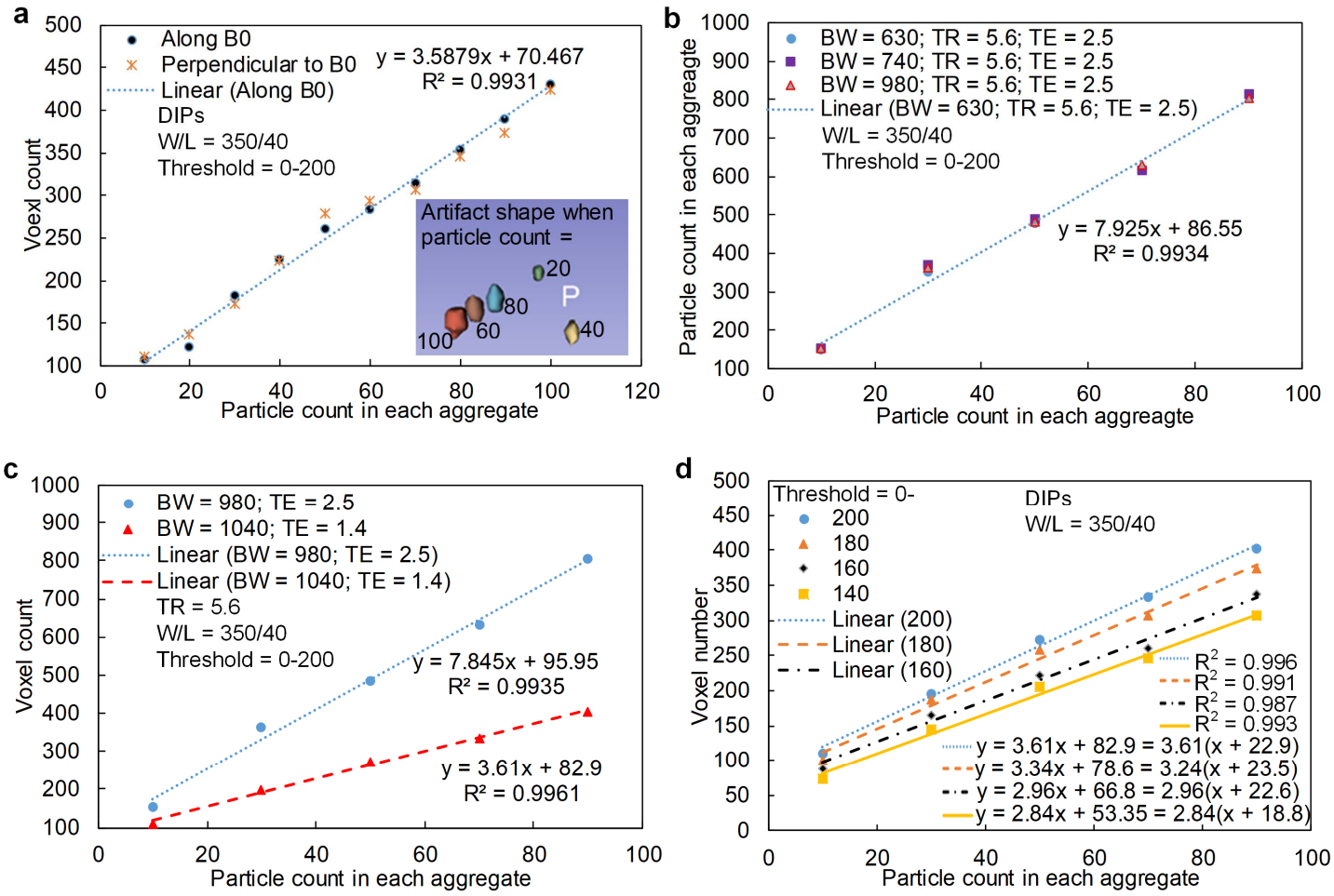

Relationship between the particle count and the corresponding artifact voxel count in the glass phantom according to orientation to B_0, BW, TE and segmentation threshold. a) The main branch of the phantom was positioned inside the MRI along and perpendicular to B_0. **b)** Particle count versus artifact voxel count when BW = 630, 740, 980, and 1040 Hz. **c)** Particle count versus artifact voxel count when using different BW (980 and 1040 Hz) and TE values (1.4 ms and 2.5 ms). **d)** Particle count versus artifact voxel count when the threshold range of the segmentation software was set to different values.

Note:1) all TR and TE values in Figures are in ms, and BW values in Hz, and 2) all parameters in this manuscript were evaluated using the OP reconstruction of the VIBE sequence.

3. Results

3.2 *In vitro* validation of hypotheses in the PVA phantom

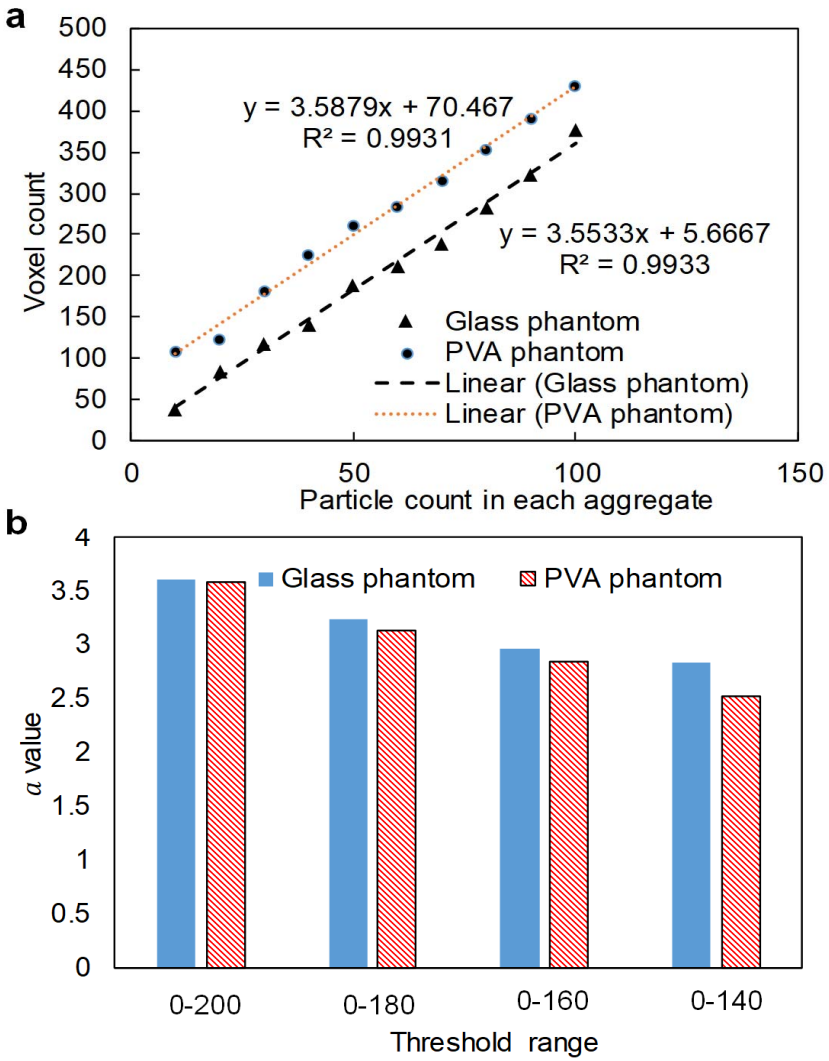

Relationship between the particle count and the corresponding artifact voxel count in the glass phantom and the PVA phantom. a) Relationship equations when only changing phantoms. **b**) Values of a in the PVA phantom and the glass phantom, when using different threshold ranges in the analysis software.

3. Results

3.3 Quantification and localization of particles in the liver of a living pig

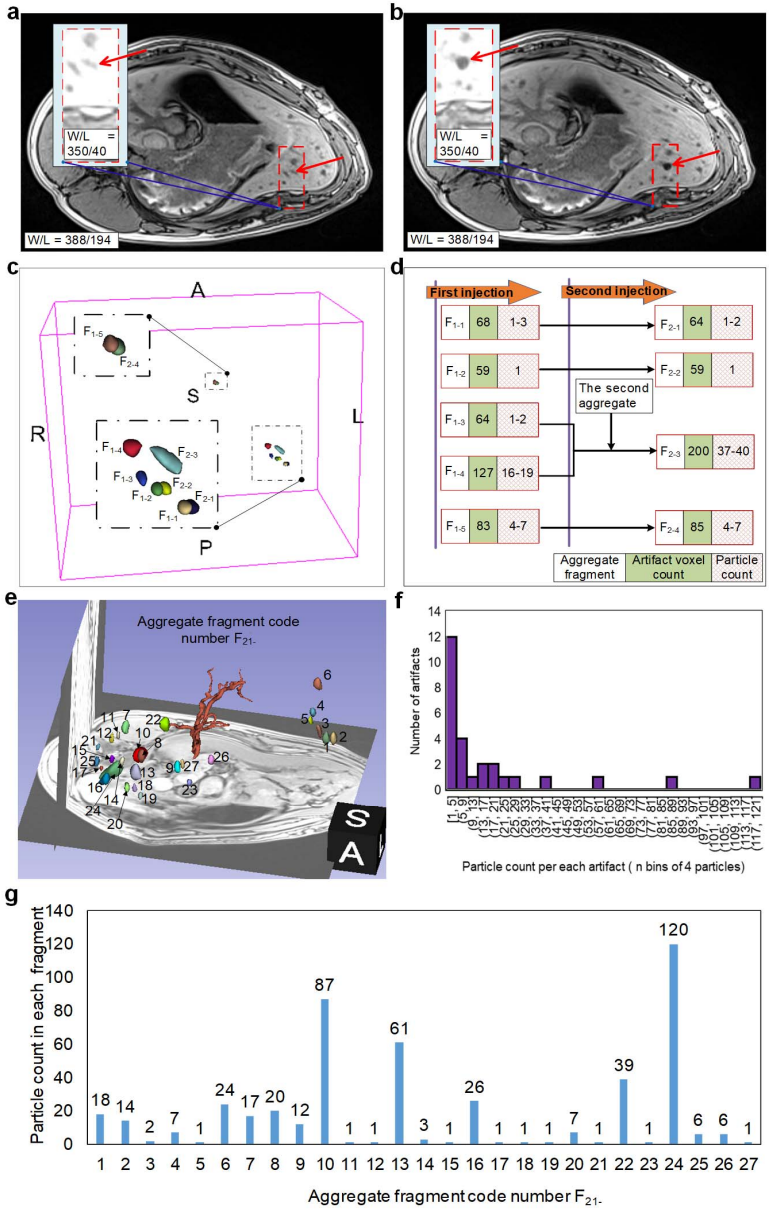

Quantification of particles in the liver of a living pig. ***In vivo*** **identification of an MDEB aggregate artifact in the liver by comparing MR images obtained (a) before and (b) after injection. c)** 3D distribution of artifacts from fragmented particle aggregates after the first two injections. **d)** Statistics of particle count in each fragment after the first two injections and using Equation ($N_v = an + b$), a = 3.6 and b = 58-67. **e)** In-vivo identification of MDEB artifacts in the liver after injecting 21 aggregates and performing magnetic resonance angiography (MRA) of hepatic arteries. f) Statistic of the particle count ranges in aggregate fragments after using Equation ($N_v = an + b$), a = 3.6 and b = 60. The code number of aggregate fragments has been marked in (**e**). **g)** Number of particles in each aggregate fragment after injecting 21 aggregates.

Note:1) a was set to 3.6 according to *in vitro* results, and 2) b value was calculated based on particle count (25 ± 6 particles) of the first aggregate injection, the obtained voxel count, and Equation ($N_v = an + b$).

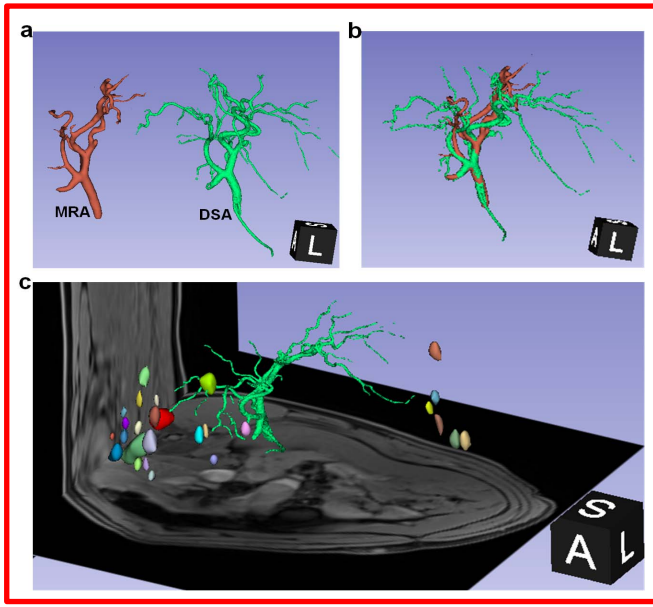

Localization of aggregate fragments in the liver. a) Hepatic arterial tree obtained by MRA and digital subtraction angiography (DSA). The hepatic tree obtained DSA is in green to facilitate identification. **b)** Coordinate alignment of the MRA and DSA images clearly displays the deformation of the hepatic vascular tree. **c)** Identification of MDEB artifacts after inserting DSA of hepatic arteries.

4. Conclusion

1. A typical **MEDBs** (200 ± 12 μm), consisting of PLGA and C12-bisphosphonate coated Fe_3O_4 nanoparticles (12 ± 3.6 nm), were successfully made, based on the physiological conditions and biocompatibility requirements for liver embolization.

2. The **targeted injection of MEDBs into the liver of a living pig** was achieved with the help of an MRI-compatible particle injection system and the MRN technology.

3. We have verified that the **volumetric interpolated breath-hold examination (VIBE) sequence**, a radio-frequency-spoiled 3D gradient-echo GRE sequence, was the **best choice** for the **quantification and 3D localization of MDEBs** in several candidates.

4. We have evaluated in-vitro the correlation between the signal loss due to magnetic particles and the acquisition parameters and segmentation technique to define a **model to predict the count of particles based on the observed signal loss** on MRI.

5. **Both particle quantification and localization were validated in the pig liver**. Results show that the proposed estimation method can identify individual MEDBs in the body. Furthermore, given the T1-VIBE sequence of MRI can be used to form high-quality multiplanar and 3D reconstruction images, it could accurately locate the 3D positions of MDEBs.

6. The techniques presented herein could become **standard methods of the accurate quantification and 3D localization of MDEBs** after navigation using different types of magnetic targeting methods or technique.

Thank you for your attention !